Infrared phonon anomalies and orbital ordering in single-crystalline MnV_2O_4 spinel

K. Myung-Whun,[1,2] S. Y. Jang,[3] T. Katsufuji,[4] and A. V. Boris[1]

[1]*Max-Planck-Institut für Festkörperforschung, Heisenbergstraβe 1, 70569 Stuttgart, Germany*

[2]*Department of Physics and IPIT, Chonbuk National University, Jeonju 561-756, Korea*

[3]*Department of Physics and Astronomy, Seoul National University, Seoul 151-747, Korea*

[4]*Department of Physics, Waseda University, Tokyo 169-8555, Japan*

(Received 2 July 2011; revised manuscript received 29 January 2012; published 20 June 2012)

We used infrared ellipsometry to study phonons in a spinel MnV_2O_4 single crystal. At 300 K, the imaginary part of the complex dielectric function spectra show four phonon peaks. Below the cubic-tetragonal structural transition temperature at 58 K, small peaks appear around the cubic modes and the number of phonons becomes more than 12. The group analysis predicted 12 infrared modes for the $I4_1/a$ symmetry. The observed modes support the $I4_1/a$ or lower crystal symmetry, which reflects the antiferro ordering of V^{3+} t_{2g} orbitals.

DOI: 10.1103/PhysRevB.85.224423 PACS number(s): 75.30.−m, 75.50.Gg, 63.20.D−, 77.22.Ch

I. INTRODUCTION

Spinel compounds have attracted interest due to the possibility of large degeneracy of magnetic ground state triggered by geometrical frustration.[1] These materials have a high propensity to break the degeneracy by a slight distortion coming from the coupling between lattice and magnetic interactions.[2] The broken degeneracy results in lowering of the symmetry reflected in the lattice dynamics. A recent infrared phonon study of $ZnCr_2O_4$ demonstrated that an antiferromagnetic spin ordering can be reconciled with the spinel lattice by a lattice distortion that relieves the geometrical frustration through a spin-Peierls-like phase transition.[3] The temperature-dependent evolution of the phonon anomalies can therefore provide us with a comprehensive insight into the microscopic understanding of the spin-lattice coupling.

In addition to the spin, the orbital degree of freedom makes the frustrated state even more complex in some spinel compounds. In MnV_2O_4, for example, the V ions devise a spinel lattice that can provoke geometrical frustration. Two electrons ($S = 1$) of the V^{3+} ion occupy the t_{2g} orbitals. Accompanying the Jahn-Teller distortion of the VO_6 octahedron, one electron occupies one of the triply degenerate t_{2g} orbitals and the other electron fills the remaining orbitals in many different ways. Since the orbital occupancy controls the strength and the sign of the magnetic exchange interaction between neighboring V spins, the frustrated orbital occupancy can cause large degeneracy of the magnetic ground state. However, depending on the emphasis of the interaction Hamiltonian, the orbitals can order with various symmetries, i.e., ferro-orbital ordering or antiferro-orbital ordering according to the theoretical studies.[4–6] As a result, the long-range ordering of the orbitals can break the degeneracy.

Information about the orbital ordering therefore should be reflected on the spin ordering and the local lattice symmetry. In MnV_2O_4, it has been revealed by neutron scattering experiments that the paramagnetic spin state changes into the collinear ferrimagnetic spin-ordered state of Mn spins ($S = 5/2$) around 61 K and the collinear ferromagnetic ordering of V spins becomes noncollinear below 58 K as the temperature decreases.[7–9] The cubic lattice at high temperature changes to a tetragonal lattice at 58 K, and an $I4_1/a$ symmetry has been suggested for the low-temperature lattice based on x-ray scattering analysis.[10] Referring to the results, theoretical studies have proposed some possible orbital ordering states.[11,12] Furthermore an antiferro-orbital ordering ground state has been proposed to be involved in the Raman-scattering process based on the intensity analysis of the Raman phonons.[13]

In addition to the experimental and theoretical studies, infrared phonon analysis can be complementary to determine the proper orbital ordering ground state. Because of the orbital-lattice coupling, a specific orbital ordering results in characteristic local crystal symmetry, and the number of infrared-active phonon modes should be determined by the local crystal symmetry. Based on this idea, Jung *et al*. have recently demonstrated that a thorough analysis of the phonon anomalies can provide valuable information about the orbital ordering in spinel oxides by examining the infrared reflectivity spectra of polycrystalline ZnV_2O_4.[14]

In this paper, motivated by the successful approach of Jung *et al*. for ZnV_2O_4, we report the temperature-dependent complex infrared dielectric function spectra of a MnV_2O_4 single crystal. Comparing with the group analysis, we determined the local crystal symmetry at low temperature and discussed the orbital ordering state.

II. EXPERIMENTS

A MnV_2O_4 single crystal was grown using a floating zone method. The structural, magnetic, and specific heat properties of the single crystals are reported elsewhere.[7,8,10] For the ellipsometry measurements, the crystal surface was polished to optical grade using a diamond suspension. Temperature-dependent infrared ellipsometry measurements were taken using a homebuilt rotating-analyzer-type variable angle ellipsometer installed at the infrared (IR1) beamline of the ANKA synchrotron light source at Karlsruhe Institute of Technology, Germany. The angle of incidence was chosen to be 70° for sample orientations with one of the axes of the cubic lattice in the plane of incidence. The sample was mounted on a cone shaped cold finger of a helium-flow cryostat.

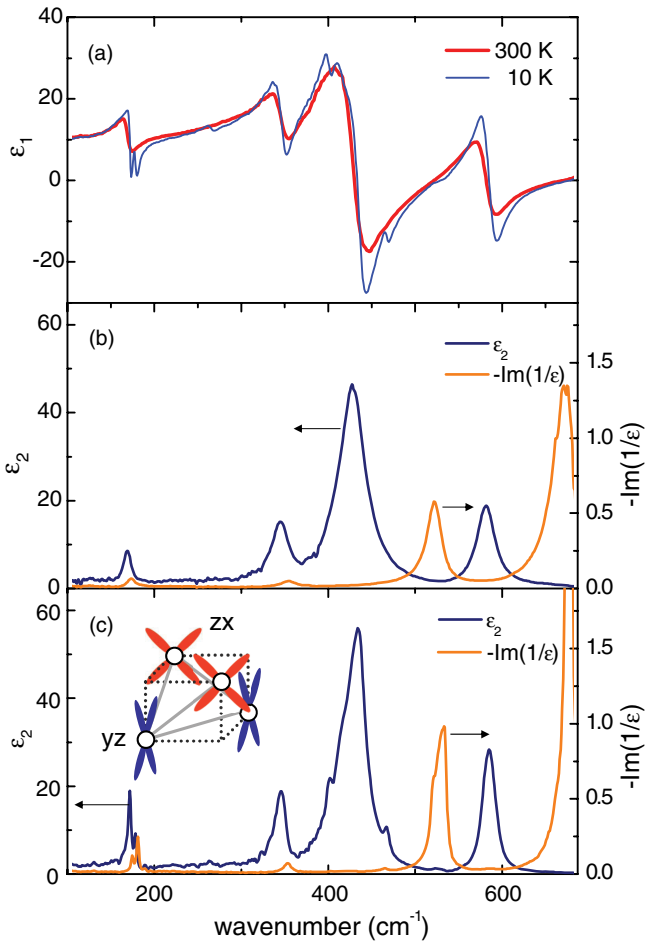

FIG. 1. (Color online) (a) Real part of the complex infrared dielectric function spectra (ε_1) at 300 K (thick solid line) and at 10 K (thin solid line). Imaginary part of the dielectric function spectra (ε_2) and the loss function [$-\mathrm{Im}(1/\varepsilon)$] (b) at 300 K and (c) at 10 K. Inset shows the schematic figure of a possible antiferro-orbital ordering of the zx and yz orbitals.

III. RESULTS

The complex infrared dielectric function (ε) reveals the signature of phonon modes. Figure 1(a) shows ε_1, the real part of the dielectric function, and Fig. 1(b) shows ε_2, the imaginary part at 300 K. Four peaks of ε_2 indicate the transverse optical (TO) phonon modes. The peak center frequencies are approximately 168, 344, 427, and 581 cm^{-1}, respectively. Figure 1(b) also shows the dielectric loss function [$-\mathrm{Im}(1/\varepsilon)$]. Four peaks correspond to the longitudinal optical (LO) phonon modes. The center frequencies are approximately 171, 352, and 521 cm^{-1}. The frequency of the highest peak is at $\sim$685 cm^{-1}, which could not be determined accurately because of the measurement limit.

Small peaks appear near the cubic lattice modes below the cubic-tetragonal lattice structure transition temperature, 58 K. Figure 1(c) shows ε_2 and $-\mathrm{Im}(1/\varepsilon)$ at 10 K. Because of the structure transition, optical anisotropy was suspected. The dielectric functions of two orthogonal surfaces of the crystal were measured and compared above and below 58 K. Significant anisotropy was not observed for this measurement within the measurement error.

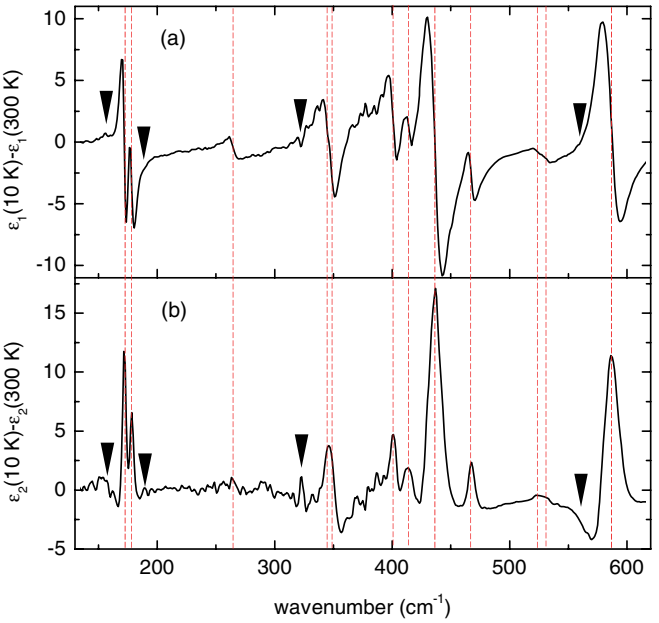

FIG. 2. (Color online) (a) Difference between ε_1 measured at 10 K and ε_1 measured at 300 K, and (b) difference between ε_2 measured at 10 K and ε_2 measured at 300 K are shown to elucidate the position of the phonons. The dotted vertical lines indicate the TO phonon modes.

To establish a guideline for analyzing the change of phonon modes at low temperature, the ε spectra at 300 K were subtracted from those at 10 K. Figures 2(a) and 2(b) show the result of $\varepsilon_1(10\ \mathrm{K}) - \varepsilon_1(300\ \mathrm{K})$ and $\varepsilon_2(10\ \mathrm{K}) - \varepsilon_2(300\ \mathrm{K})$, respectively. The N-shape feature in ε_1 and the peak in ε_2 at the same frequency indicate the appearance of new modes or the change of the existing modes. The vertical dashed lines mark the probable phonon mode positions. The result suggests that more than 12 phonon modes should be assigned at 10 K. There are also weak modes marked by the inverted triangles.

To identify the phonon modes more accurately, careful fitting with the oscillators was attempted. For the fitting, the factorized oscillator model shown below was used:[15]

$$\varepsilon(\omega) = \epsilon_\infty \prod_j \frac{\omega_{\mathrm{LO}j}^2 - \omega^2 - i\gamma_{\mathrm{LO}j}\omega}{\omega_{\mathrm{TO}j}^2 - \omega^2 - i\gamma_{\mathrm{TO}j}\omega}. \quad (1)$$

Here ϵ_∞ is the dielectric constant at high frequency. $\omega_{\mathrm{LO}j}$, $\omega_{\mathrm{TO}j}$, $\gamma_{\mathrm{LO}j}$, and $\gamma_{\mathrm{TO}j}$ represent the LO and TO phonon mode frequency and damping constant of the jth mode, respectively. Four oscillators were used to fit the 300 K data, and thirteen oscillators were used to fit the 10 K data. Small peaks noted by solid triangles were not counted in the fitting. The fitting parameters are summarized in Table I.

Figure 3(a) shows the temperature dependence of ε_2 near the 168 cm^{-1} TO mode. The 300 K peak remains almost unchanged until 70 K. Around 70 K, weak peaks appear at 181 and 170 cm^{-1}, indicated by solid arrows, and they become more apparent below 60 K. In addition to the small peaks counted in the fitting, weak peaks at 130 and 150 cm^{-1}, a shoulderlike structure at 163 cm^{-1}, and a weak structure at 188 cm^{-1} marked by the open arrows appear at low temperatures. Those peaks were not considered in the fitting analysis because of their weak strength.

TABLE I. Oscillator fitting parameters at 300 and 10 K. The error bars are shown in Fig. 4. The unit of the parameters is cm^{-1}.

Temperature	ω_{TO}	γ_{TO}	ω_{LO}	γ_{LO}
300 K	168	9	171	9
	344	19	352	20
	427	37	521	19
	581	22	685	21
10 K	172	4	175	3
	178	3	181	3
	264	9	265	10
	343	17	350	30
	353	18	354	9
	402	9	404	7
	412	22	421	30
	434	25	467	8
	468	7	520	8
	522	10	529	13
	534	12	536	6
	578	13	579	18
	586	19	690	30

Figure 3(b) shows the temperature dependence near the 344 cm^{-1} TO mode. The 300 K peak becomes sharper and slightly asymmetric with decreasing temperature. One oscillator was used to fit the peak at high temperature ($\gtrsim$100 K), but the peak was not well fit with one oscillator because of the asymmetric shape at low temperatures. Two oscillators were assigned to fit the peak shape properly below 80 K as marked by the solid arrows. A small peak at 325 cm^{-1},

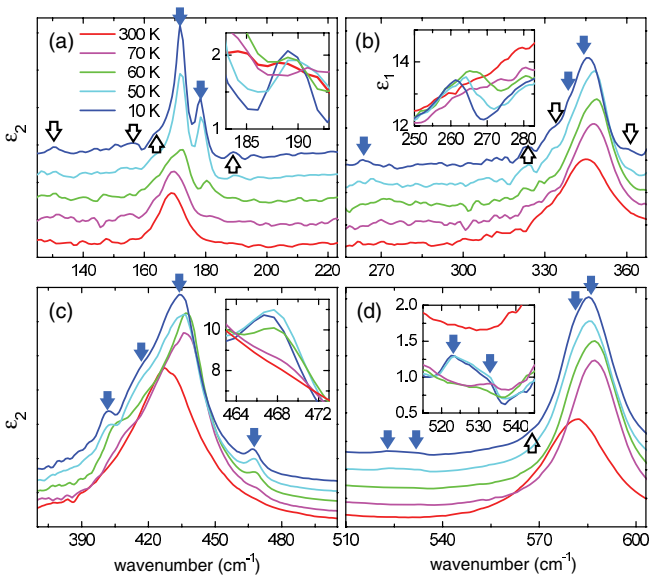

FIG. 3. (Color online) Temperature dependence of ε_2 around the four major phonon modes. The data were shifted by some constant for separating the curves. The inset in Fig. 3(b) shows the real part of the dielectric function spectra ε_1 near 260 cm^{-1} and the insets in Figs. 3(c) and 3(d) magnify the spectra near 465 and 580 cm^{-1}, respectively. The data of insets were not shifted. The solid arrows mark the peak center frequencies of the oscillator modes used in the fitting. The open arrows denote the weak peaklike structures, which were not considered in the oscillator fitting.

a shoulderlike structure at 330 cm^{-1}, and a weak peak structure at 362 cm^{-1} marked by the open arrows also appear below 60 K, but they were not considered in the fitting.

A small peak also appeared near 264 cm^{-1}. It was not clear in the ε_2 spectra. However, the *N*-shape structure pointing out a phonon mode appears clearly in the ε_1 spectra at temperatures of 60 K and below, as shown in the inset of Fig. 3(b).

Figure 3(c) shows the temperature dependence near the 427 cm^{-1} TO mode. The 300 K peak becomes enhanced asymmetrically with decreasing temperature and additional peaks appear as marked by the solid arrows below 70 K. The 402 cm^{-1} peak moves to approximately 400 cm^{-1} as the temperature decreases, so it becomes clearly separated from the main peak below 60 K. The 412 cm^{-1} peak also moves to a lower frequency and appears as a shoulder structure. Another small peak appeared at 470 cm^{-1} at 70 K. The peak shape becomes clear at 60 K and below, as shown in the inset in Fig. 3(c).

Figure 3(d) shows the temperature dependence of ε_2 near the 581 cm^{-1} TO mode. The peak intensity and its frequency increases with decreasing temperature. The peak becomes asymmetric at low temperatures. Large asymmetric enhancement of the phonon peak intensity at low temperatures could not be fit with one oscillator, so two oscillators were used for proper fitting. The intensity enhancement leading to an asymmetric line is interpreted as peak splitting due to the symmetry reduction. The splitting, however, occurs at a much higher temperature ($\gtrsim$100 K) than the structural phase transition temperature (58 K), which indicates that the splitting is not simply due to the lattice structural symmetry change. In addition, a small structure appears around 530 cm^{-1} as shown in the inset of Fig. 3(d). This structure is negligible in the 60 K data, but it abruptly appears in the 55 K data (not shown, but almost the same as the 50 K data). To fit the structure, at least two oscillators (denoted by solid arrows) were needed because of the asymmetric shape.

The TO phonons at 300 K were separated and their frequencies shifted oppositely to higher or lower frequencies, as summarized in Fig. 4. The phonon mode split reflects the lattice symmetry change and should be mainly due to the cubic-tetragonal structural phase transition at 58 K. The phonon mode split can be categorized by the temperature dependence. The small peaks shown in Figs. 4(a) and 4(e) appeared just around the structural transition temperature. On the other hand, the other small peaks between 300 and 600 cm^{-1} shown in Figs. 4(b)–4(d), and 4(f) appeared at high temperatures as high as 80 K, well above the structural transition temperature.

The temperature dependence of TO phonon frequency was compared with a simple model describing the pure anharmonic effect,

$$\omega(T)_j = \omega_{0j}\left(1 - \frac{c_j}{\exp(\Theta/T) - 1}\right). \quad (2)$$

Here, $\omega(T)_j$ is the frequency of the jth TO mode at temperature T, and ω_{0j} is the jth TO phonon frequency at 0 K. c_j is the fitting parameter determining the strength of the anharmonic contributions.[16,17] Θ is the Debye temperature determined from an arithmetic average of the four room-temperature phonon frequencies. The solid lines in Fig. 4 correspond to the

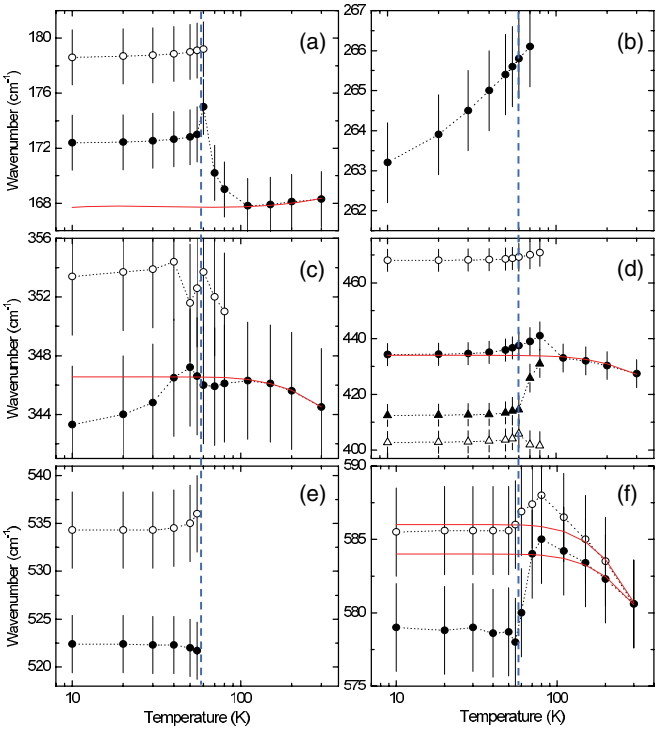

FIG. 4. (Color online) Semilogarithmic plot for the temperature dependence of the vibrational mode frequencies obtained from the oscillator fitting. The vertical dotted lines represent the cubic-tetragonal structural phase transition temperature $T_S = 58$ K. The solid lines correspond to the expected anharmonic temperature dependence of TO mode frequencies as calculated according to Eq. (2).

theoretical anharmonic temperature dependence of TO mode frequencies. These curves were derived by fitting the high temperature ($T \geqslant 150$ K) values of the phonon frequencies and Θ was 380 K. There are strong frequency shifts in the phonon modes from normal anharmonic behavior. These shifts appear well above the onset of the magnetic ordering temperature (61 K) and the structure transition temperature (58 K, the dotted vertical lines).

The frequencies of the 168 cm^{-1} mode [Fig. 4(a)] reveal positive shift compared to normal anharmonic behavior. The 344 cm^{-1} mode [Fig. 4(c)] exhibits negative shifts when entering the low-temperature phase. The main peaks of the 427 [Fig. 4(d)] and 581 cm^{-1} modes [Fig. 4(f)] show similar behaviors. They show positive shift around the transition temperatures and a negative deviation from the anharmonic dependence below the transition temperatures.

IV. DISCUSSION

An estimate based on the analogy with $ZnCr_2O_4$ was attempted to understand the temperature dependence, although the phonon frequencies and the local lattice symmetry of $ZnCr_2O_4$ are not exactly matched with those of MnV_2O_4. According to the calculation for $ZnCr_2O_4$ phonons at room temperature, it is reasonable to consider that the 168 cm^{-1} phonon mode frequency of MnV_2O_4 is determined mainly from force constants of Mn-O vibration. The 344 cm^{-1} mode can be determined mainly from force constants of V-V and V-O vibrations. The 427 and 581 cm^{-1} mode frequencies are mostly influenced by the force constants of V-O vibration.[18] Magnetic interaction between the neighboring ions can cause the frequency of a phonon mode to be shifted from its cubic state value because of the spin-phonon coupling.[19] The positive frequency shift of the 168 cm^{-1} phonon mode from simple anharmonic behavior indicates vibrational force constant enhancement for the low-temperature spin-ordered phase, which can be due to the antiferromagnetic Mn-O exchange interaction. Similarly, the 344 cm^{-1} mode frequency shift can be understood as the result of competition between the V-spin direct exchange and the V-O superexchange. The 427 and 581 cm^{-1} mode frequency shifts can be the result of the force constant change due to the V-O superexchange.

The spin ordering can also induce the phonon mode split. The phonon mode split survives higher temperatures above 58 K. This may be due to the local lattice structure fluctuation. However, some small peaks appear even above 80 K, which cannot be attributed to the structural fluctuation. It is more reasonable to consider that the spin ordering can induce a large lattice anisotropy in the phonon frequency with large split occurring for cubic phonon modes as suggested in $ZnCr_2O_4$ study.[19] The split can occur at high temperatures above the long-range ferrimagnetic ordering temperature (61 K) if the short-range fluctuation of the magnetic ordering survives high temperatures. Neutron scattering experiment studies reported the signature of large magnetic-moment fluctuation at high temperatures above 100 K.[20,21] This suggests the possible relation between the phonon split and the magnetic ordering, but further studies are desirable to understand the shift and split of phonon mode frequency clearly.

The number of phonon modes at 10 K reflects the crystal symmetry and the orbital ordering state. Four modes are observed at room temperature, but the number increases to more than 13 at low temperatures. If the small peaks not counted in the fitting are included, more than 21 peaks are observed below 60 K. As summarized in Table II, the group analysis suggests four infrared active modes ($4T_{1u}$) for the cubic symmetry ($Fd\bar{3}m$). The four modes of cubic lattice split into doublets of eight modes under the tetragonal lattice symmetry. The silent modes in the cubic symmetry become infrared active by the symmetry change. A ferro-type orbital ordering in the tetragonal lattice accompanies the $I4_1/amd$-type symmetry for which the group analysis predicts ten infrared-active modes. An antiferro-type orbital ordering accompanies the $I4_1/a$-type symmetry for which the group analysis predicts 12 infrared-active modes. The observed modes suggest that the V-t_{2g} orbitals in MnV_2O_4 prefer an antiferro-type ordering of $I4_1/a$ symmetry or even lower

TABLE II. Infrared (IR) active phonon modes derived from a group theoretical analysis. The translational modes are excluded.

Symmetry (space group, point group)	IR phonon mode
Cubic ($Fd\bar{3}m$, O_h)	T_{1u} (four modes)
Tetragonal ($I4_1/amd$, D_{4h})	A_{2u} (four modes)
	E_u (six modes)
Tetragonal ($I4_1/a$, C_{4h})	A_u (six modes)
	E_u (six modes)

symmetry. The inset of Fig. 1(c) shows a possible ordering pattern of V-t_{2g} zx and yz orbitals schematically following the suggestion of Suzuki *et al.*[10]

However, it is also possible that some of the small peaks are not only due to the lattice phonon. The electromagnon or electro-two-magnon modes were observed in some multiferroic materials where the spins form some noncollinear structures.[22,23] Multiferroic properties were not observed, but the V-spin ordering structure is noncollinear in MnV_2O_4. Because of the spin structure the local electric polarization ($\vec{P}_{ij}$) can be generated by the interaction between the neighboring spins $\vec{S}_i$ and $\vec{S}_j$ along their connecting unit vector $\vec{e}_{ij}$. According to the neutron scattering and the theoretical calculation, $\vec{P}_{ij}$ proportional to $\vec{e}_{ij} \times (\vec{S}_i \times \vec{S}_j)$ is finite,[8,24] which suggests that the spin-induced local polarization is possible. Spin-wave modes were observed below 250 cm^{-1} by a neutron scattering experiment.[8] A theoretical study predicted a magnon excitation in the Raman spectra.[24] Raman-scattering experiment study suggested that a few modes between 178 and 306 cm^{-1} arise from magnetic excitations.[13] Under these assumptions, the magnetic excitations can be infrared active and some of the small peaks of dielectric functions in the corresponding energy range can be also due to the magnon modes. Even if the magnetic excitation contribution is excluded, there are still more than 12 phonon modes, which suggests that the low-temperature symmetry is close to $I4_1/a$ type and the V-ion orbital can prefer the antiferro-type orbital ordering. Further theoretical, studies taking into account of both spin and orbital degrees of freedom are desirable to assign all the peaks in the dielectric functions observed.

V. CONCLUSION

By using the spectroscopic ellipsometry technique four phonon modes were observed at room temperature in the dielectric function spectra and more than 12 phonon modes were observed at low temperatures, which suggests that the ground-state symmetry of MnV_2O_4 is $I4_1/a$ or lower and the V-t_{2g} orbitals may prefer an antiferro-type orbital ordering.

ACKNOWLEDGMENTS

We thank Y.-L. Mathis for the support at ANKA. K.M.-W. acknowledges the Alexander von Humboldt foundation, Chonbuk National University Research Fund, and the National Research Foundation of Korea (NRF Grant No. 2009-0069982 and No. 220-2011-1-C00016).

[1] P. G. Radelli, New J. Phys. **7**, 53 (2005).
[2] S.-H. Lee, D. Louca, M. Matsuda, S. Ji, H. Ueda, Y. Ueda, T. Katsufuji, J.-H. Chung, S. Park, S.-W. Cheong, and C. Broholm, J. Phys. Soc. Jpn. **79**, 011004 (2010).
[3] A. B. Sushkov, O. Tchernyshyov, W. Ratcliff, S. W. Cheong, and H. D. Drew, Phys. Rev. Lett. **94**, 137202 (2005).
[4] Y. Motome and H. Tsunetsugu, Phys. Rev. B **70**, 184427 (2004).
[5] O. Tchernyshyov, Phys. Rev. Lett. **93**, 157206 (2004).
[6] S. Di Matteo, G. Jackeli, and N. B. Perkins, Phys. Rev. B **72**, 020408(R) (2005).
[7] Kim Myung-Whun, J. S. Kim, T. Katsufuji, and R. K. Kremer, Phys. Rev. B **83**, 024403 (2011).
[8] J. H. Chung, J. H. Kim, S. H. Lee, T. J. Sato, T. Suzuki, M. Katsumura, and T. Katsufuji, Phys. Rev. B **77**, 054412 (2008).
[9] V. O. Garlea, R. Jin, D. Mandrus, B. Roessli, Q. Huang, M. Miller, A. J. Schultz, and S. E. Nagler, Phys. Rev. Lett. **100**, 066404 (2008).
[10] T. Suzuki, M. Katsumura, K. Taniguchi, T. Arima, and T. Katsufuji, Phys. Rev. Lett. **98**, 127203 (2007).
[11] S. Sarkar, T. Maitra, R. Valenti, and T. Saha-Dasgupta, Phys. Rev. Lett. **102**, 216405 (2009).
[12] Gia-Wei Chern, Natalia Perkins, and Zhihao Hao, Phys. Rev. B **81**, 125127 (2010).
[13] K. Takubo, R. Kubota, T. Suzuki, T. Kanzaki, S. Miyahara, N. Furukawa, and T. Katsufuji, Phys. Rev. B **84**, 094406 (2011).
[14] Sung Hoon Jung, JaeHoon Noh, Jooyun Kim, C. L. Zhang, S.-W. Cheong, and E. J. Choi, J. Phys.: Condens. Matter **20**, 175205 (2008).
[15] We used the software packages developed by B. P. Gorshunov and S. Schultz, WASF program, 1, Physikalisches Institut, Universitt Stuttgart, Germany and by A. Kuzmenko, REFFIT software package, University of Geneva [http://optics.unige.ch/alexey/reffit.html].
[16] T. Rudolf, Ch. Kant, F. Mayr, J. Hemberger, V. Tsurkan, and A. Loidl, Phys. Rev. B **76**, 174307 (2007).
[17] Ch. Kant, J. Deisenhofer, T. Rudolf, F. Mayr, F. Schrettle, A. Loidl, V. Gnezdilov, D. Wulferding, P. Lemmens, and V. Tsurkan, Phys. Rev. B **80**, 214417 (2009).
[18] J. Himmrich and H. D. Lutz, Solid State Commun. **79**, 447 (1991).
[19] C. J. Fennie and K. M. Rabe, Phys. Rev. Lett. **96**, 205505 (2006).
[20] R. Plumier and M. Sougi, Solid State Commun. **64**, 53 (1987).
[21] J. H. Chung (private communication).
[22] R. Valdés Aguilar, A. B. Sushkov, C. L. Zhang, Y. J. Choi, S.-W. Cheong, and H. D. Drew, Phys. Rev. B **76**, 060404(R) (2007).
[23] Y. Takahashi, N. Kida, Y. Yamasaki, J. Fujioka, T. Arima, R. Shimano, S. Miyahara, M. Mochizuki, N. Furukawa, and Y. Tokura, Phys. Rev. Lett. **101**, 187201 (2008).
[24] S. Miyahara, K. Takubo, T. Suzuki, T. Katsufuji, and N. Furukawa, arXiv:1012.4073v1.